Use of Synthetic Aperture Radar and Uncrewed Aerial Vehicle for Assessing Pavement Condition

Amit Gajurel, S.M.ASCE[1]; Nripojyoti Biswas, Ph.D.[2]; Hiramani Chimauriya, S.M.ASCE[3]; and Anand J. Puppala, Ph.D., P.E., F.ASCE[4]

[1]Doctoral Candidate, Zachry Dept. of Civil and Environmental Engineering, Texas A&M Univ., College Station, TX. Email: amitgajurel@tamu.edu
[2]Senior Research Engineer, Zachry Dept. of Civil and Environmental Engineering, Texas A&M Univ., College Station, TX. Email: nripojyoti.biswas@tamu.edu
[3]Doctoral Candidate, Zachry Dept. of Civil and Environmental Engineering, Texas A&M Univ., College Station, TX. Email: hiramani12@tamu.edu
[4]A.P. and Florence Wiley Chair Professor, Zachry Dept. of Civil and Environmental Engineering, Texas A&M Univ., College Station, TX. Email: anandp@tamu.edu

ABSTRACT

The long-term monitoring of transportation infrastructure assets, such as pavements, highway embankments, and earth retaining systems, at a lower cost, and with short mobilization time, is of interest to owners and stakeholders. Due to the improvement in spatial and temporal resolution of synthetic aperture radar (SAR) remote sensing systems as well as the drastic reduction in the price of data acquisition, SAR has now become a viable method to provide an economical and rapid condition assessment of transportation assets. This paper presents an example of this through a case study on the inspection and characterization of a pavement surface based on the amplitude of backscattering from an X-band radar. In situ characterization of the test site was first performed using aerial photogrammetry techniques with uncrewed aerial vehicle (UAV). The pavement features, extracted from the digital twin model created using photogrammetry, were compared with the radar cross section (RCS) of the pavement. The results show that problematic areas evident during in situ characterization can be delineated and quantified based on the normalized radar cross-section of the pavement surface. Overall, the outcomes of this research demonstrate the potential of SAR for future transportation asset management undertakings and can be of significant interest to state engineers and practitioners.

Keywords: Remote Sensing, Synthetic Aperture Radar (SAR), Transportation Assets, Uncrewed Aerial Vehicle (UAV)

INTRODUCTION

Transportation assets are an indispensable and intricate system of infrastructures that provide an efficient and safe mode of transit for goods and people. Timely monitoring and maintenance of these assets is of major interest as they support and contribute abundantly to the day-to-day lives of billions of people. The average age of transportation assets has been increasing – indicating a deterioration in asset condition in the long run (USDOT 2021, 2023). The Transportation Asset Management (TAM) plan mandates state Department of Transportations (DOTs) to annually and/or biennially inspect certain assets – bridges and pavement, and encourages inspection of other assets – walls, slopes, embankments, and subgrades within the

pavement Right-of-Way (ROW). The primary goal of TAM is to maintain physical assets at an acceptable level over its lifecycle at minimum cost to the stakeholders. Among many assets, pavements and bridges have been the primary focus of transportation agencies including those in the south-central states. Such focus has indeed improved the condition of the higher functioning pavements and bridges since 2000 (USDOT 2021, 2023). Besides pavement and bridges, geotechnical assets - such as walls, slopes, embankments, and subgrades, within its vicinity have a significant effect on the lifecycle of a transportation system. However, the lack of data on inventory, condition data, and performance measures of assets other than pavement and bridges on NHS limits the scope for TAM applications.

Recent years have seen a significant boom in space-borne remote sensing platforms like Synthetic Aperture Radar (SAR) satellites in both public and private sectors. Such rapid development has resulted in free access to large archives of medium resolution data– with global coverage every 6 - 12 days, and significant drop in image acquisition cost for high-resolution data (ICEYE 2023; Ignatenko et al. 2020; Torres et al. 2012). Unlike traditional optical sensors, SAR can collect data irrespective of weather conditions, cloud cover, and the presence of sunlight. Such data have a potential to be used for rapid and on-demand condition assessment and performance monitoring of transportation assets. Data from SAR can be utilized to effortlessly extend the current TAM scope as well as increase the monitoring frequency of assets as needed. Recent studies have shown that these sensor can be used to obtain data during inclement weather, natural disasters, and other hazard events (Ardila et al. 2022; Kourkouli 2023). The continued development of SAR satellite constellation has made possible capabilities like monitoring an asset at a given area multiple times in a single day with up to 0.5 m ground resolution irrespective of illumination from sunlight and weather conditions (Paek et al. 2020). This advancement is also accompanied by a sharp decrease in data acquisition and processing costs. These developments make it possible to closely monitor transportation systems, quickly identify distress, and swiftly deploy countermeasures that aid in preserving existing assets and enhancing service life.

Advancement in digital sensors for taking images and storage technology enabled capturing numerous high resolution images affordable in mid to late 2000s. FM is a photogrammetric method used in UAVs to generate high resolution 3D structures for a series of overlapping images that is typically derived from moving sensor (Snavely et al. 2008). Scale and rotation invariant key features are identified in each of these overlapping image which are then used to estimate camera pose and scene geometry to extract point cloud in image-space (Snavely et al. 2008; Westoby et al. 2012). The 3D point clouds are transformed to real-world co-ordinate system using Ground Control Points (GCPs) during the post-processing step. Redundant network of these evenly distributed GCPs, which are high-contrast targets both in field and point cloud, is established to account to any potential issues with sparse data or errors in SfM reconstruction (Congress et al. 2018; Westoby et al. 2012).

In this study, the authors illustrate an application of high-resolution X-band SAR data for analyzing pavement surfaces, utilizing backscattering amplitude as the primary metric. The methodology involves a comprehensive in-situ assessment of the pavement utilizing advanced aerial photogrammetry using Uncrewed Aerial Vehicles (UAVs) platform. This process generated a digital twin model of the pavement, from which specific features are extracted and subsequently correlated with the radar cross-section data of the same surface. The findings of this research highlight the ability to identify and quantify problem areas on the pavement, as detected during the in-situ evaluation, by analyzing the normalized radar cross-section. The

implications of this study are significant, demonstrating the utility of Synthetic Aperture Radar (SAR) in the field of transportation asset management. This research holds considerable relevance for state engineers and professionals in the field, underscoring the potential benefits of SAR technology in future infrastructure maintenance and management projects.

SYNTHETIC APERTURE RADAR (SAR)

SAR sensors are imaging radars that operate at microwave range, i.e., the wavelength of 0.75 cm to 120 cm, and provide unique information about the incident surface which is distinct from conventional optical and infrared images (Moreira et al. 2013). Unlike passive sensors, which rely on external sources of radiation like sunlight, SAR systems actively transmit electromagnetic waves and measure the backscatter from various surface features. The transmitter generates successive bursts of the chirped pulse at regular intervals which are focused by the antenna into a beam. The beam illuminates the surface obliquely in the direction right angle to the flight line (also known as range direction) and the SAR sensor system receives a portion of the transmitted energy. This is used to obtain the Radar Cross Section (RCS) – the inferred target area based on the ratio of the received response signal intensity and transmitted signal intensity. For a given wavelength and observation angle, RCS is dependent on the physical properties, such as geometry and roughness, and electrical properties, such as the dielectric constant of the incident surface. Depending on the type/orientation of the area used to normalize, a number of RCS measures are estimated. Radar brightness (β^0) is the quantity measured by a SAR sensor which is equal to RCS normalized with a solid rectangle defined in the slant range plane representing the ground surface. The Normalized Radar Cross Section (NRCS), also known as sigma nought (σ^0) is calculated by normalizing RCS with an actual geometrical area on the ground surface. σ^0 is the primary value of interest to the image analyst as it quantifies the ground surface response and minimizes the radiometric difference with change in incidence angles, acquisition geometry, and look direction (Small 2011; Woodhouse 2006). For this study, the equation used for calculating σ^0 is given by Equation 1 – calibration equation from provided by Capella Space (Capella Space 2022).

$$\sigma^0_{\mathrm{dB}} = 20 \log_{10}(\mathrm{SC} * \mathrm{DN}_{\mathrm{geo}}) \quad (1)$$

Where,

σ^0_{dB} = Normalized Radar Cross section (NRCS) (m^2/m^2) in dB scale

SC = Scale factor provided in the metadata for each scene

$\mathrm{DN}_{\mathrm{geo}}$ = UInt16 raster value of the image

The radar response of surfaces like pavement, low-vegetation fields, and bare soils is dominated by surface scattering – which is the main contributor to the NRCS. Surface scattering is primarily the function of the roughness of the surface, the wavelength of the SAR sensor, and the incidence angle. Therefore, for a given wavelength and incidence angle of the SAR sensor, the roughness of the surface becomes the main contributing factor for the radar response of pavements and alike surfaces.

One of the criteria to classify the smoothness or roughness of a surface with respect to the incident electromagnetic wave is the Fraunhofer roughness criterion given by Equation 2 (Jensen 2014; Ulaby and Long 2014; Woodhouse 2006). This criterion is useful in modeling the scattering and emission behavior of natural surfaces in the microwave region where the

wavelength (λ) is of the same order as that of the root mean square (rms) height of the surface. It is calculated based on the formula shown in Equation 3. In this study, the SAR system is a X-band (λ = 3.1 cm) radar with incidence angle (θ) of 30.6º. Substituting these values in Equation 3, shows that for s < 0.11 cm, the surface can be considered smooth.

$$s < \frac{\lambda}{32\cos(\theta)} \tag{2}$$

$$s = \left[\frac{1}{N-1}\sum_{i=1}^{N} z_i^2 - N\bar{z}^2\right]^{\frac{1}{2}} \tag{3}$$

Where,
s = rms height
λ = wavelength of electromagnetic wave
θ = incidence angle
N = number of samples
$\bar{z_i} = \frac{1}{N}\sum_{i=1}^{N} z_i$
z_i = Height profile of the surface in consideration

The rms heights (roughness) from UAV platform as well as mean NRCS data (radar response) from SAR satellite were extracted for analysis. The analysis was performed for 0.5 m segment length.

CASE STUDY: PAVEMENT IN RELLIS CAMPUS, BRYAN, TX

The site for this case study was the Proving Grounds Research Facilities located at the 2,000-acre RELLIS Campus of Texas A&M University System in Bryan, Texas. This facility contains multiple runways, aprons, and transportation-related pavements. This study includes RTA Zone 2 35C Sect 3 as shown in Figure 1.

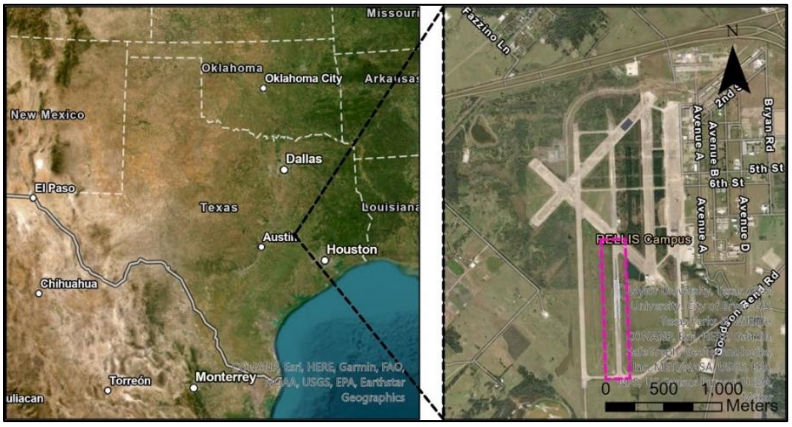

Figure 1: Location of the study site at RELLIS Campus in Texas A&M University

Digital twin model. UAV was used to collect high-resolution aerial images of the site as shown in Figure 2(a). A reconnaissance survey of the site was used to finalize the flight plan and locations of the ground control points. Data acquisition was performed using the UAV platform

equipped with an optical sensor, Real Time Kinematics (RTK) navigation system, and Post Processing Kinematics (PPK) geotagging system. The GPS information of each image from the UAV platform was corrected using the data from the PPK system after flight. Similar processes have been used by several researchers in correcting the GPS coordinate post-flight (Congress and Puppala 2022; Thomas et al. 2020; Zhang et al. 2019). The images with corrected GPS information and Ground Control Points (GCPs) were ingested into a SfM photogrammetry software to generate dense point cloud, Digital Surface Model (DSM), and ortho-mosaic. DSMs and ortho-mosaics were exported to GIS environments for creating 3D models and extracting elevation data. DSM overlain by the ortho-mosaic facilitated the creation of a digital twin model of the site with a spatial resolution of 0.49 cm Figure 2(b).

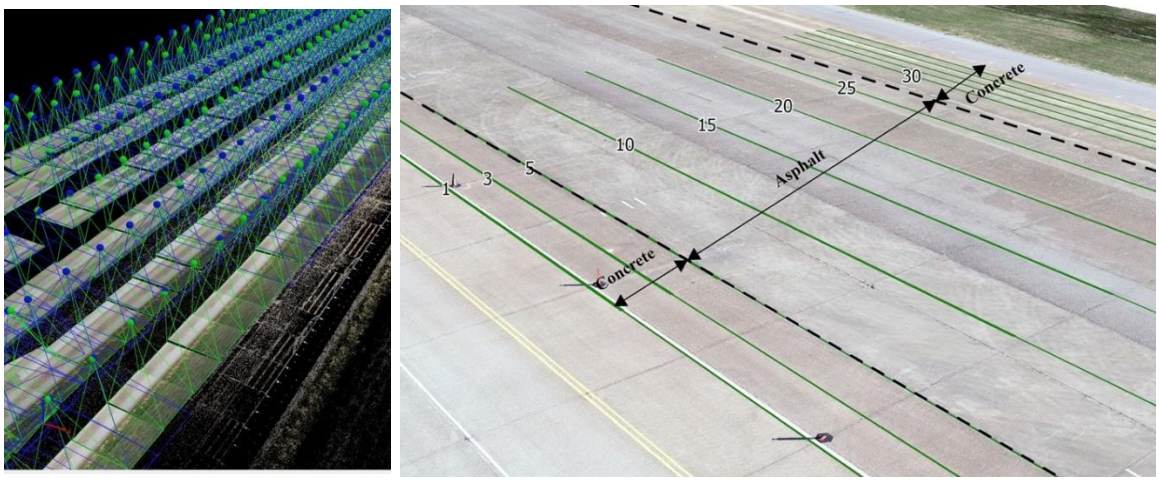

(a) **(b)**

Figure 2: UAV data of the site (a) dense point could generation (b) digital twin

The pavement elevation profiles along a 200 m long stretch of the sections labelled in Figure 2(b) were extracted using ENVI. The rms value along these sections are computed using Equation 3 for segment length of 0.5 m. for both concrete and asphalt pavement sections.

High resolution SAR. Satellite tasking, data acquisition, and download of high-resolution SAR data was performed through Capella Space® for the RELLIS campus (Figure 3). Spotlight Geocoded Terrain Corrected (GEO) SAR data product downloaded for this site is a one dimensional raster, where each pixels has been calibrated for radar internal subsystems and corrected for location (Capella Space 2022). The imagery was imported into a GIS environment and calibrated to obtain a raster with NRCS in decibels (dB) scale. Geo-referencing of the SAR data was performed using 1st-order affine transformation to correctly align the SAR data. NRCS along the profile sections corresponding to the digital twin section were extracted.

RESULTS AND DISCUSSION

The NRCS value in dB is plotted against the rms (in cm.) value along the profile (both concrete and asphalt surfaces) for segment length of 0.5 m to access relationship between them. Figure 4, Figure 6, and Figure 7 shows the comparison between NRCS value and rms value for the concrete pavements on either side of the central asphalt pavement. Figure 5 and Figure 6 shows similar comparison between profile sections on the asphalt pavement. It is evident that the

rms value, calculated from the digital twin model do not show variation among different pavement types whereas the NRCS of the pavement surface shows variation. This suggests that SAR data can capture the subtle surface texture difference between asphalt and concrete pavements. This is clearly visible in the case of comparison of NRCS value along Line 10, 15, 20, and 25 (which are all asphalt pavements) with other sections. In case of Line 25, the pavement surface looks aged and has early signs of alligator cracks along its length in comparison to other asphalt pavement (shown in Figure 8) – which in turn has higher value of NRCS. Although the NRCS is higher, the rms value of the surface remains unaffected by these distresses. This suggests that initiation of pavement failure with distress like alligator cracking are visible with SAR data at its early stages than with measuring surface profiles. The concrete pavements, as visible in the orthomosaics, do not show any visible deterioration and seem to be in good condition. Therefore, the rms value of the surface is consistently low in all the profiles. For a concrete pavement without any visible surface distresses, the NRCS value of the surface had a mean value of -18.6 dB with standard deviation of 1.4 dB. This suggests that using an X-band radar a good concrete pavement can be identified. Similarly, for an asphalt pavement without any visible surface distresses, the mean NRCS value of -15.8 dB with standard deviation of 1.5 dB. Likewise, for line 25 (shown in Figure 8), the average NRCS value if -13.5 dB with standard deviation of 1.6 dB.

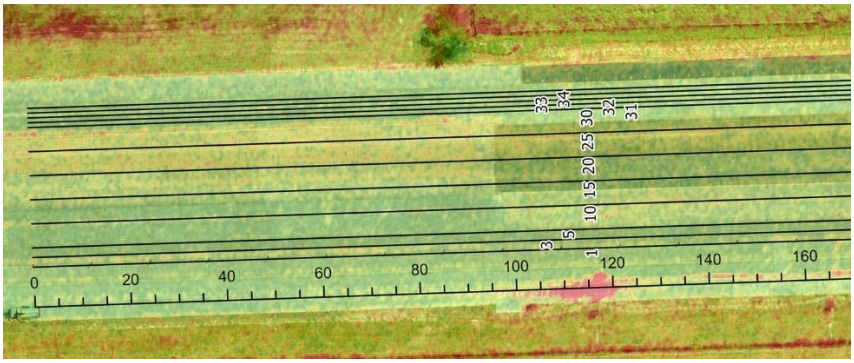

Figure 3: Location of profile sections overlain by SAR amplitude data

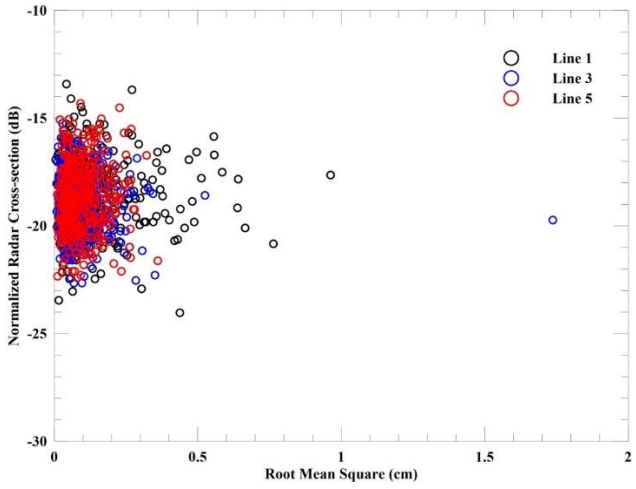

Figure 4. NRCS vs rms value for 0.5 m segment length for Line 01, 03, and 05

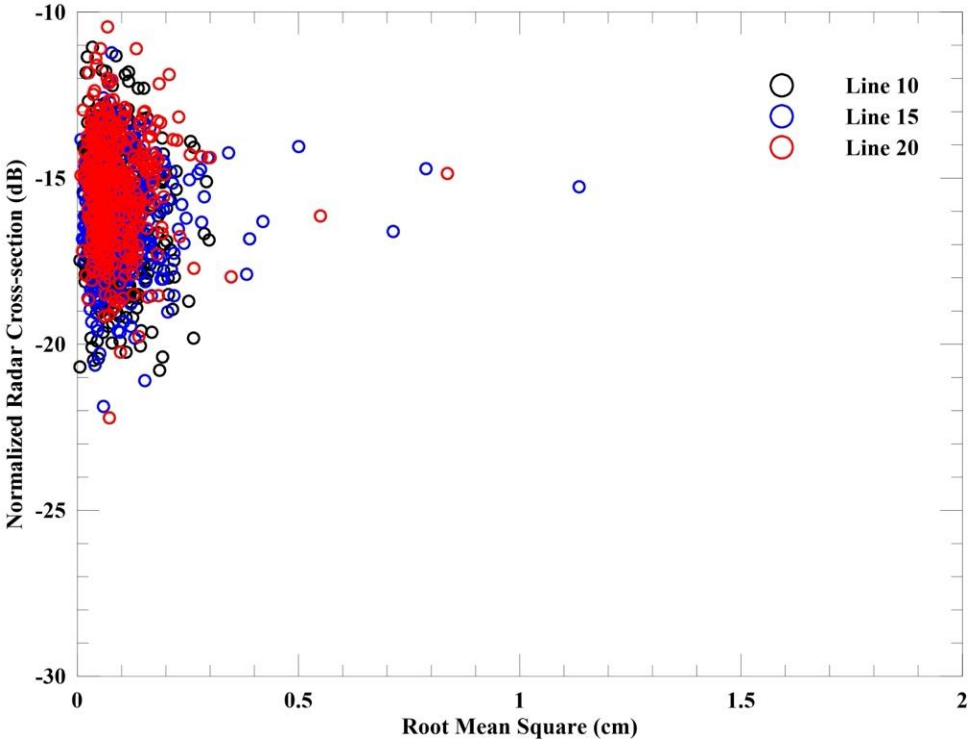

Figure 5. NRCS vs rms value for 0.5 m segment length for Line 10, 15, and 20

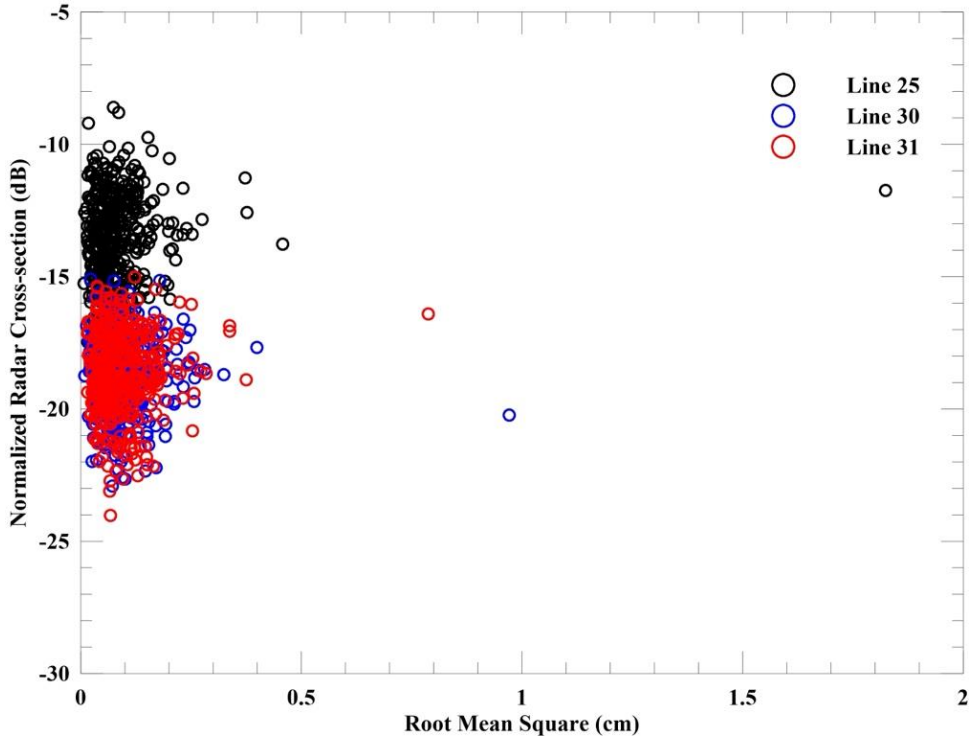

Figure 6. NRCS vs rms value for 0.5 m segment length for Line 25, 30, and 31

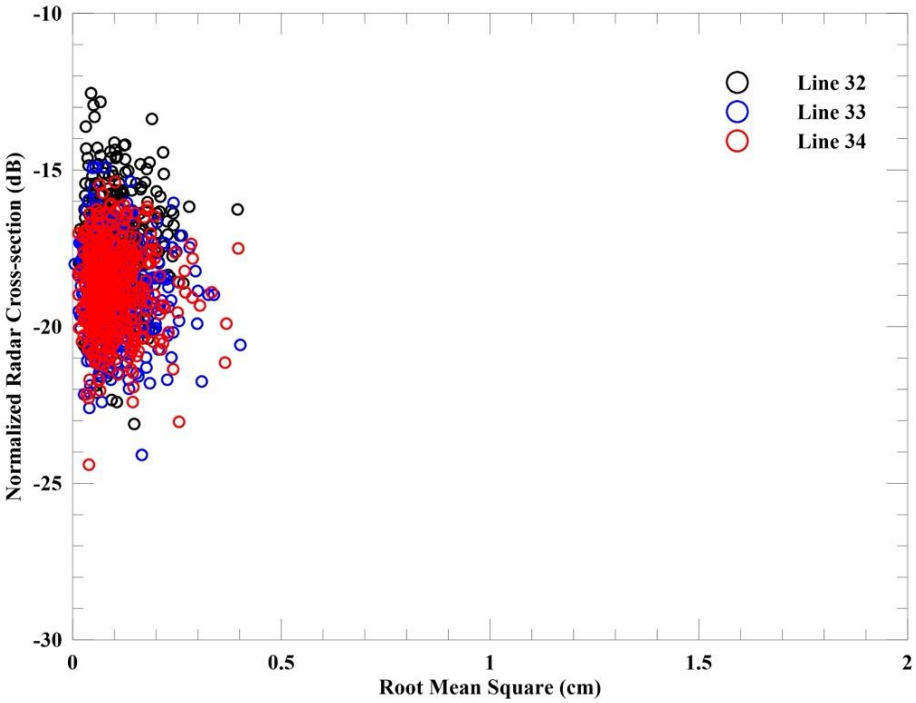

Figure 7. NRCS vs rms value for 0.5 m segment length for Line 32, 33, and 34

Figure 8. Early-stage alligator cracks present along Line 25

CONCLUSIONS

The study showcased a noteworthy relationship between the NRCS values and the surface profiles of various pavement types. Even though rms values derived from the digital twin model didn't display a significant distinction between different pavements, the NRCS distinctly captured the subtle differences in surface texture between concrete and asphalt pavements. Key findings include:

- The analysis distinctly highlighted how SAR data can recognize early signs of pavement failures, such as alligator cracking, even when there aren't noticeable variations in the rms values.
- The concrete and asphalt pavements appeared to be in good condition with consistent but different rms values, underlining the robustness of X-band SAR data.
- By employing an X-band radar, it is possible to identify the spatial location and condition of good concrete and asphalt pavements based on their respective mean NRCS values.
- High resolution X-band SAR data can be a reliable tool for detecting early signs of pavement distress and for characterizing the integrity of different pavement materials.

REFERENCES

Ardila, J., P. Laurila, P. Kourkouli, and S. Strong. 2022. "Persistent Monitoring and Mapping of Floods Globally Based on the Iceye Sar Imaging Constellation." *IGARSS 2022-2022 IEEE International Geoscience and Remote Sensing Symposium*, 6296–6299. Kuala Lumpur, Malaysia: IEEE.

Capella Space. 2022. "Capella Space Synthetic Aperture Radar (SAR) Open Dataset." Accessed November 22, 2022. https://registry.opendata.aws/capella_opendata.

Congress, S., and A. Puppala. 2022. "Eye in the sky: Condition monitoring of transportation infrastructure using drones." *Proceedings of the Institution of Civil Engineers: Civil Engineering*, 1–9.

Congress, S. S. C., A. J. Puppala, and C. L. Lundberg. 2018. "Total system error analysis of UAV-CRP technology for monitoring transportation infrastructure assets." *Engineering Geology*, 247: 104–116.

ICEYE. 2023. "Satellite Data - How to use satellite data for better decision making." Accessed April 30, 2023. https://www.iceye.com/satellite-data.

Ignatenko, V., P. Laurila, A. Radius, L. Lamentowski, O. Antropov, and D. Muff. 2020. "ICEYE Microsatellite SAR Constellation Status Update: Evaluation of First Commercial Imaging Modes." *IGARSS 2020-2020 IEEE International Geoscience and Remote Sensing Symposium*, 3581–3584. Waikoloa, HI, USA: IEEE.

Jensen, J. R. 2014. *Remote sensing of the environment : an earth resource perspective*. Pearson.

Kourkouli, P. 2023. "Natural disaster monitoring using ICEYE SAR data." *Geoinformatics for Geosciences*, 163–170. Elsevier.

Moreira, A., P. Prats-Iraola, M. Younis, G. Krieger, I. Hajnsek, and K. P. Papathanassiou. 2013. "A tutorial on synthetic aperture radar." *IEEE Geosci. Remote Sens. Mag.*, 1 (1): 6–43.

Paek, S. W., S. Balasubramanian, S. Kim, and O. De Weck. 2020. "Small-Satellite Synthetic Aperture Radar for Continuous Global Biospheric Monitoring: A Review." *Remote Sensing*, 12 (16): 2546.

Small, D. 2011. "Flattening gamma: Radiometric terrain correction for SAR imagery." *IEEE Transactions on Geoscience and Remote Sensing*, 49 (8): 3081–3093.
Snavely, N., S. M. Seitz, and R. Szeliski. 2008. "Modeling the World from Internet Photo Collections." *Int J Comput Vis*, 80 (2): 189–210.
Thomas, O., C. Stallings, and B. Wilkinson. 2020. "Unmanned aerial vehicles can accurately, reliably, and economically compete with terrestrial mapping methods." *Journal of Unmanned Vehicle Systems*, 8 (1): 57–74.
Torres, R., et al. 2012. "GMES Sentinel-1 mission." *Remote Sensing of Environment*, 120: 9–24.
Ulaby, F. T., and D. G. Long. 2014. *Microwave Radar and Radiometric Remote Sensing*. Ann Arbor: The University of Michigan Press.
USDOT. 2021. *National Transportation Statistics 2021*. Washington, DC: US Department of Transportation, Bureau of Transportation Statistics.
USDOT. 2023. *Transportation Statistics Annual Report 2022*. United States. Department of Transportation. Bureau of Transportation Statistics. Not Available.
Westoby, M. J., J. Brasington, N. F. Glasser, M. J. Hambrey, and J. M. Reynolds. 2012. "'Structure-from-Motion' photogrammetry: A low-cost, effective tool for geoscience applications." *Geomorphology*, 179: 300–314.
Woodhouse, I. H. 2006. *Introduction to Microwave Remote Sensing*. CRC Press. Boca Raton: Taylor & Francis.
Zhang, H., E. Aldana-Jague, F. Clapuyt, F. Wilken, V. Vanacker, and K. Van Oost. 2019. "Evaluating the potential of post-processing kinematic (PPK) georeferencing for UAV-based structure-from-motion (SfM) photogrammetry and surface change detection." *Earth Surface Dynamics*, 7 (3): 807–827.